HHS Public Access
Author manuscript
J Control Release. Author manuscript; available in PMC 2017 February 10.

Published in final edited form as:
J Control Release. 2016 February 10; 223: 109–117. doi:10.1016/j.jconrel.2015.12.034.

Targeted Gene Transfer to the Brain via the Delivery of Brain-Penetrating DNA Nanoparticles with Focused Ultrasound

Brian P. Mead[a], **Panagiotis Mastorakos**[b,c], **Jung Soo Suk**[b], **Alexander L. Klibanov**[a,d], **Justin Hanes**[b,*], and **Richard J. Price**[a,*]

[a]Biomedical Engineering, University of Virginia, Charlottesville, VA 22908, USA

[b]Center for Nanomedicine at the Wilmer Eye Institute, Johns Hopkins University School of Medicine, Baltimore, MD 21231, USA

[c]Department of Neurological Surgery, University of Virginia, Charlottesville, VA 22908, USA

[d]Cardiovascular Division, University of Virginia, Charlottesville, VA 22908, USA

Abstract

Gene therapy holds promise for the treatment of many pathologies of the central nervous system (CNS), including brain tumors and neurodegenerative diseases. However, the delivery of systemically administered gene carriers to the CNS is hindered by both the blood-brain barrier (BBB) and the nanoporous and electrostatically charged brain extracelluar matrix (ECM), which acts as a steric and adhesive barrier. We have previously shown that these physiological barriers may be overcome by, respectively, opening the BBB with MR image-guided focused ultrasound (FUS) and microbubbles and using highly compact "brain penetrating" nanoparticles (BPN) coated with a dense polyethylene glycol corona that prevents adhesion to ECM components. Here, we tested whether this combined approach could be utilized to deliver systemically administered DNA-bearing BPN (DNA-BPN) across the BBB and mediate localized, robust, and sustained transgene expression in the rat brain. Systemically administered DNA-BPN delivered through the BBB with FUS led to dose-dependent transgene expression only in the FUS-treated region that was evident as early as 24 h post administration and lasted for at least 28 days. In the FUS-treated region ~42% of all cells, including neurons and astrocytes, were transfected, while less than 6% were transfected in the contralateral non-FUS treated hemisphere. Importantly, this was achieved without any sign of toxicity or astrocyte activation. We conclude that the image-guided delivery of DNA-BPN with FUS and microbubbles constitutes a safe and non-invasive strategy for targeted gene therapy to the brain.

[*]Corresponding Authors: Richard J. Price, Ph.D., Department of Biomedical Engineering, Box 800759, Health System, University of Virginia, Charlottesville, VA 22908, USA, rprice@virginia.edu; Justin Hanes, Ph.D., Center for Nanomedicine at the Wilmer Eye Institute, Johns Hopkins University School of Medicine, 400 N. Broadway, 6th Floor, Baltimore, MD 21231, USA, hanes@jhmi.edu.

Author Contributions
The manuscript was written through contributions of all authors. All authors have given approval to the final version of the manuscript.

Keywords

Focused Ultrasound; Non-Viral Gene Delivery; CNS Diseases; Blood Brain Barrier

Gene therapy approaches have shown promise for the treatment of Parkinson's disease,[1-6] Alzheimer's disease,[7,8] lysosomal storage diseases[9,10] and brain tumors.[11] Viral gene vectors have been used in clinical trials for neurological disorders and shown to be therapeutically effective.[12] However, viral vectors, such as adenovirus, adeno-associated viruses and herpes simplex viruses have significant limitations, including safety concerns, limited packaging capacity, technical difficulties in scale up and high production costs.[13] Moreover, prior exposures and/or repeated administrations of these vectors lead to neutralizing immune responses that ultimately reduce the efficiency of transgene delivery.[14,15] DNA-bearing nanoparticles (DNA-NP) have emerged as a versatile and easily adaptable platform for gene therapy devoid of the aforementioned limitations.

Regardless of the type of gene vectors used, the blood brain barrier (BBB) prohibits delivery of systemically administered vectors to the central nervous system (CNS), resulting in minimal transgene expression.[16] Even specific viral vectors or DNA-NP with BBB-targeting ligands achieve only minimal accumulation in the brain when administered at very high doses, which are associated with potential adverse effects in peripheral organs.[17] For this reason, the majority of preclinical and clinical studies have focused on direct intracranial administration of gene vectors. However, the invasive nature of this approach and the risks associated with surgery limit the applicability of this strategy and its potential use for repeated administrations. Various methods for circumventing the BBB, such as intra-arterial infusion of osmotic agents, have been proposed, but they are invasive and non-targeted,[18,19] leading to transgene expression in an uncontrolled fashion.

Currently, focused ultrasound (FUS) is the only modality allowing repeated, non-invasive, and temporary BBB permeabilization, leading to localized therapeutic delivery to the brain.[20,21] Circulating ultrasound contrast agent microbubbles (MBs), when exposed to low intensity FUS, oscillate in volume with acoustic rarefaction and compression.[22] Ultimately, interactions between these activated MBs with the vascular wall lead to disruption of tight junctional complexes[23] and induction of active transport processes across the BBB.[24] Importantly, high capillary density in the brain permits many points of entry after FUS application, potentiating improved distribution compared to local injection. BBB opening is temporary, typically resolving within 4-6 h,[20,25] and has shown safety in several experimental animal models, including rhesus macaques.[26] Furthermore, both preclinical and clinical studies have demonstrated the potential of FUS to deliver systemically administered payloads including imaging agents,[27,28] ~100 nm liposomes,[29,30] ~150 kDa antibodies,[31,32] recombinant proteins,[33] ~20 nm viruses[34,35] and ~10 μm neural stem cells[36] into the brain. Toward this end, the size of BBB opening is dependent on FUS acoustic pressures[37], suggesting the FUS parameters can be tuned to accommodate delivery of therapeutics of different sizes. FUS can be aimed with guidance from magnetic resonance imaging systems, allowing for accurate targeting of predefined brain structures; devices capable of targeting ultrasound through the human skull with sub-millimeter precision are currently in clinical trials.[38,39]

Once beyond the BBB, the brain parenchyma provides an additional barrier to the diffusion of nanoparticles (NP). This brain-tissue barrier (BTB) consists of a nanoporous microstructure of negatively charged ECM macromolecules that hampers the distribution of NP[40,41] and viruses[42] via adhesive interactions and/or steric obstruction. It has recently been shown that sub-115 nm NP densely coated with neutrally charged and bio-inert polyethylene glycol (PEG) are able to overcome the BTB and rapidly diffuse within the brain tissue.[40] We have demonstrated that BBB opening with MR-guided FUS and MBs can facilitate the delivery of colloidally stable, densely PEGylated 60 nm fluorescent tracer brain-penetrating NP (BPN) across the BBB.[21] Once delivered across the BBB, BPN exhibited wide dispersion into the tissue away from the vessels of entry, allowing for homogeneous distribution in the FUS-treated tissue.

In this study, we used colloidally stable DNA-NP with a dense PEG coating (DNA-BPN) previously shown to achieve remarkable penetration through the BTB and high levels of transfection following direct intracranial administration.[43] By combining FUS-mediated BBB opening with systemically administered DNA-BPN, we formulated a non-invasive strategy to achieve safe, highly localized, robust, and sustained transgene expression in the CNS.

Results and Discussion

We formulated highly PEGylated DNA-BPN based on a gold-standard cationic polymer, polyethylenimine (PEI), as previous described.[43-45] This technique allowed the formulation of highly compact and colloidally stable 56 ± 2nm DNA-BPN with a PEG to PEI w/w ratio of 50 that is substantially higher than PEGylation ratios used traditionally[46-48]. Effective shielding of the NP positive surface charge was confirmed by the near-neutral ζ-potential (+1.5 ± 0.3 mV; Table 1). We further measured the stability of DNA-BPN in pooled human plasma (PHP; Innovative Research, Novi, MI); DNA-BPN retained their colloidal stability following incubation in PHP at 37°C, as evidenced by the well-preserved hydrodynamic diameters (65 ± 7 nm), near-neutral surface charge (−1.8 ± 0.8 mV) and polydispersity index (PDI) of 0.25 (Table 1). Despite a minimal increase in size, DNA-BPN did not aggregate, retained their sub-100 nm diameter and DNA compaction over at least 30 min of incubation in PHP at 37°C, as demonstrated by the hydrodynamic diameter histograms and transmission electron micrographs (Figure 1a, b). This may be attributed to the inclusion of free PEI in the formulation of BPN allowing the formation of strongly positive polymer core that leads to efficient DNA compaction in spite of the steric hindrance imposed by the use of dense amounts of PEG.

To measure the *in vivo* transfection efficiency of DNA-BPN, we formulated DNA-BPN with a plasmid containing a luciferase reporter gene driven by a long-acting β-actin promoter (pBAL). These DNA-BPN were intravenously co-injected at 3 different concentrations (50 μg, 100 μg and 200 μg) with MBs in Sprague-Dawley rats (n = 5 per dose) and FUS was applied to the striatum of the left hemisphere. Gene expression was measured using an *In*

Vivo Imaging System (IVIS100; Xenogen, Alameda, CA). FUS-mediated BBB permeabilization led to targeted DNA-BPN delivery to the brain and robust bioluminescence at the ultrasound focus (i.e. anatomical location where FUS was applied) (Figure 2a). Bioluminescence was not detected in brain tissue outside of the FUS focal region. Furthermore, extending the IVIS scan to include the entire rat revealed that transgene expression was not detectable in any other off-target organs, including the liver (Figure S1). However, we acknowledge the possibility that more sensitive approaches could show some limited expression in off-target organs. Such studies will be important when specific applications of this approach are indicated. *Ex vivo* bioluminescent imaging was also performed on freshly excised brains at day 28 after DNA-BPN administration in order to confirm that the *in vivo* transfection measurements were not due to signal from extra-axial tissues such as the skin and/or the skull (Figure 2b). *Ex vivo* images offer higher resolution and thus confirmed luciferase transgene expression through the entire ultrasound focus without off-target transgene expression. Repeated IVIS imaging demonstrated persistent dose-dependent reporter transgene expression for at least 28 days. Of note, even the lowest DNA-BPN dose led to bioluminescence signal significantly above the background (Figure 2c, d). Importantly, gene expression was observed as early as 24 hours after FUS-mediated delivery of DNA-BPN. Compared to commonly used viral vectors, this constitutes a very short lag time. [49] Some viral vectors (e.g. AAV2) require up to 5 weeks to achieve maximal expression, [50] indicating that their expression kinetics are less favorable than that of DNA-BPN. Importantly, expression persistence represents a marked improvement over previously published results using non-viral gene vectors. For example, in a study wherein MB bound pDNA was delivered across the BBB with FUS, expression dropped to ~10% of maximum after just 14 days.[51]

We next determined the transfection efficiency and neuron-astrocyte tropism following FUS-mediated delivery of DNA-BPN. We used DNA-BPN containing an mCherry plasmid driven by the β-actin promoter (pBACH). The hydrodynamic diameter (56±2 nm) and ζ-potential (1.5±0.3 mV) of these pBACH-carrying DNA-BPN were consistent with those of DNA-BPN complexed with pBAL. One week after FUS mediated delivery of pBACH bearing DNA-BPN, whole-brain *ex vivo* epifluorescence imaging confirmed mCherry transgene expression in the FUS-targeted region (Figure 3a). Microscopic examination of the FUS-targeted regions of nuclear counterstained (Draq5) brain cross-sections (Figure 3b) yielded visually detectable levels of mCherry expression, even at the lowest DNA-BPN dose. DNA-BPN achieved efficient transfection throughout the ultrasound focus region, in good agreement with a previous study suggesting the ability of densely PEGylated DNA-BPN to distribute homogeneously throughout brain parenchyma.[43] At the 200 μg DNA-BPN dose, 42.3% of cells in the ultrasound focus expressed the transgene compared to only 5.8% in the non-FUS treated contralateral hemisphere (Figure 3c). The population of cells transfected by the 200 μg dose was significantly greater than the transfection efficiency of 30.2% or 28.0% found at the 100 μg or 50 μg doses, respectively. Consistent with our results generated using pBAL, mCherry gene expression appeared to be dose dependent (Figure 3c, n=6 per dose). Furthermore, we confirmed that transgene expression is directly dependent on FUS treatment because, even at a very high DNA-BPN dose, transgene expression beyond the intact BBB of the contralateral hemisphere was minimal. The highly efficient transfection of a large cell population within the FUS focus is most likely attributed to the contribution of FUS to improving DNA-BPN penetration through the BBB,[44] as well as the widespread distribution of DNA-BPN within the brain tissue. This is in good agreement with previous findings in which ultrasound enhanced delivery and transfection efficiency in FUS-treated tissue following systemic administration of NP.[52,53] In fact, ultrasound mediated delivery of pBAL bearing NP, similar to the formulation used in the current study, led to strong and localized expression in hard-to-transfect skeletal muscle *in vivo*,[44] even greater than the level achieved by direct injection.

To then determine which cell types are transfected with this approach, additional cross-sections were immunolabeled for NeuN (neuronal marker), GFAP (astrocyte marker), and mCherry (Figure 4). DNA-BPN vectors entered both astrocytes and neurons in FUS-targeted tissue (Figure 4a). Out of the transfected neuron-astrocyte cell population, approximately 42% of transfected cells were neurons and the remaining 58% of transfected cells were astrocytes (Figure 4B, n = 6).

Numerous gene therapy studies have shown the importance of restricting transgene expression to particular cell types. Cell-specific transgene expression can be achieved by the use of specific promoters. For example, transgene expression in the brain can be limited to astrocytes with a GFAP promoter[54] or neurons with a synapsin[55] or MeCP2[56] promoter.

Neurotrophic factors including glial cell line-derived neurotrophic factor (GDNF), which has been shown to be neuroprotective in models of neurodegenerative disease[57], is produced primarily by a subset of neurons in the striatum[58]. For this reason, several groups have pursued neuronal specific gene therapies[55]. However, several other studies have demonstrated a prominent role of astrocytes in neurodegenerative disease progression[59,60] and astrocyte proliferation has been observed in models of neurodegeneration[61]. Moreover, astrocyte populations have been shown to increase 2-4 fold over the lifetime of rodents,[62] while neuronal populations are declining. Astrocyte-specific overexpression of neurotrophic factors leads to similar therapeutic efficacy as neuron-derived expression.[54] Non-viral vectors such as the DNA-BPN used in the current study have the advantage of allowing remarkable versatility for gene delivery applications. Broad cellular tropisms will allow greater control at the gene level to restrict transgene expression to the target cells.

FUS has previously demonstrated the ability to improve efficiency of several different gene vectors in the brain after systemic administration. While self-complementary adeno-associated virus 9 (scAAV9) broadly transfects cells beyond the BBB even without additional targeting mechanisms, doses as high as ~1×10^{11} vg/g have been found to transduce only 19% of motor neurons in adult mice.[63] Delivery of scAAV9 into the brain[34] or spinal-cord[64] with FUS achieved almost 80% total transduction efficiency in the brain and 87% of neurons in the spinal cord at 2.5 $\times10^9$ or 2×10^9 vg/g, respectively. While scAAV9 currently yields higher transfection than DNA-BPN in the brain after delivery with FUS, scAAV9 has a packaging capacity of just 2.4 kb[65], which may limit the versatility of this vector for some applications. Indeed, tailorability, high packaging capacity and ease of manufacture make non-viral gene vector systems enticing, and further optimization of DNA-BPN formulation may enhance efficiency in the CNS.

FUS has recently been shown to mediate transgene expression in mouse brain after delivery of relatively large (i.e. ~100 nm diameter) non-viral liposomal-based gene vectors [66]. Although transfection efficiency was not reported, luciferase co-localized with neurons and astrocytes [37]. To deliver these relatively large liposomes across the BBB, a FUS frequency of 500 KHz was used with a peak-negative pressure of 0.5 MPa. While reactive gliosis was not assessed, H&E staining did reveal that some petechiae were evident [37]. In contrast, our smaller diameter (56 + 2 nm) brain penetrating gene-vectors were delivered across the BBB with FUS [i.e. 1 MHz frequency with 0.6 MPa peak-negative pressure to a species with a much thicker skull (rats)] and MBs without creating petechiae or gliosis. Our study also differs in that our mCherry reporter studies reveal that combining these relatively small vectors with a near-neutral (+1.5 ± 0.3 mV) surface chargepotentiateshomogeneous dispersion through FUS-targeted tissue. Furthermore, we demonstrated that this system provides robust transgene expression for at least 28 days as opposed to 4 days.

Finally, we histologically examined brain tissues for signs of toxicity and/or gliosis. Hematoxylin and eosin (H&E) stained brain tissues that had been transfected via the delivery of DNA-BPN with FUS-mediated BBB opening were used to assess local toxicity (Figure 5 a); comparisons were made to contralateral control hemispheres (i.e. FUS^{-}, DNA-BPN^{+}) and animals receiving no treatment. Importantly, no cellular damage was observed at any dose in either the FUS-treated or contralateral control hemispheres. Hemosiderin staining was found in the FUS treated region in only 2 of the n=18 brains tested. When examined as fraction of tissue area coverage, less than 0.1% of the observed H&E stained tissue area was hemosiderin positive, thereby indicating that erythrocyte leakage across the BBB after FUS treatment was an exceptionally rare occurrence. GFAP immunolabeling was used to assess potential astrocyte activation (i.e. gliosis) (Figure 5a). Comparisons of average grayscale intensity in GFAP stained images across several depths in the brain revealed that GFAP staining intensity was unchanged when compared to both the contralateral region (i.e. FUS−, DNA-BPN+) and untreated controls (FUS−,DNA-BPN-). This indicates that no long-term astrocyte activation occurred in response to DNA-BPN delivery via FUS-mediated permeabilization of the BBB (Figure 5b, n=6 per group). We also note that no long-term changes in animal behavior were observed following FUS-mediated delivery of DNA-BPN.

While the long term safety of BBB opening with FUS and MBs has been confirmed in animals through both tissue histology and animal behavior tests, it is also well known that driving MBs beyond a mode of stable cavitation and into an inertial cavitation mode can lead to blood pooling in tissue.[67,68] Nonetheless, inertial cavitation is avoidable and it has been argued that minor erythrocyte extravasation would have minimal impact[27,69] and such minor effects would be acceptable in treatments of diseases like tumors or neurodegenerative disease. With regard to PEI, its high positive charge density has raised concerns about toxicity.[48] In particular, non-PEGylated PEI NP have been shown to lead to cell death *in vitro* and *in vivo* after intracranial administration[43,70]. However, when the surface of PEI-based NP are densely coated with PEG, such as with the DNA-BPN used in the current study, toxicity is negligible.[43] Our safety results are consistent with those reported for convection enhanced delivery of PEI-based DNA-BPN, wherein no vector-induced toxicity was observed at high doses in rats.[43]

In conclusion, we provide here the first demonstration of targeted, robust, and sustained CNS transfection achieved by delivering systemically administered DNA-BPN across the BBB with FUS and MBs. This platform approach for gene delivery to the CNS has potential as a targeted and non-invasive modality for treatment of a variety of neurological diseases, including brain tumors and neurodegenerative diseases.

Materials and Methods

Animals

Female Sprague-Dawley rats were purchased from Harlan and maintained on a 12/12h light/dark cycle. Rats used in the experiments weighed between 180-220 g and were given food and water *ad libitum*. All animal experiments were approved by the Animal Care and Use Committee at the University of Virginia and conformed to the National Institutes of Health regulations for the use of animals in research.

DNA-BPN Fabrication and Characterization

To synthesize a PEG_{5k}-PEI copolymer, methoxy-PEG-N-hydroxysuccinimide (mPEG-NHS; 5 kDa; Sigma-Aldrich, St. Louis, MO) was conjugated to 25 kDa branched PEI (Sigma-Aldrich), as previously described (PEG_{5k}-PEI)[43-45]. Nuclear magnetic resonance (NMR) was used to confirm a PEG: PEI ratio of 50; a ratio previously shown to provide sufficient shielding of the DNA-NP positive surface charge[43]. ^{1}H NMR (500 MHz, D2O): δ 2.48 – 3.20 (br, CH2CH2NH), 3.62 – 3.72 (br, CH2CH2O). The pBAL and pBACH plasmids were produced by Copernicus Therapeutics Inc. (Cleveland, OH). DNA-NP were formulated by the drop-wise addition of 10 volumes of plasmid DNA (0.2 mg/ml) to 1 volume of polymer solution with a PEI concentration of 0.38 mg/ml and PEGPEI concentration of 1.17 mg/ml. PEI solutions were prepared at a previously optimized nitrogen to phosphate (N/P) ratio of 6 and at PEG_{5k}-PEI to PEI molar ratio of 3. This resulted in formulation of NP with a DNA: PEI: PEG-PEI ratio of 1:0.1:0.6 and a DNA:polymer ratio of 1:0.7. This ratio allows the administration of high DNA amounts (50 μg, 100 μg or 200 μg) while limiting the amount of polymer administered (35 μg, 70 μg, 140 μg respectively). Gene vectors were washed with 3 volumes of ultrapure water, and concentrated to 1 mg/ml using Amicon® Ultra Centrifugal Filters (100,000 MWCO; Millipore Corp., Billerica, MA) so as to remove free polymers. DNA concentration was determined using a NanoDrop ND-1000 spectrophotometer (NanoDrop Technologies, Wilmington, DE).

To characterize DNA-NP in water as well as PHP we used a Nanosizer ZS90 (Malvern Instruments, Southborough, MA). Hydrodynamic diameter and PDI were measured in 10 mM NaCl at pH 7.0 by dynamic light scattering (DLS); ζ-potential was similarly measured by laser Doppler anemometry. In order to determine the DNA-NP morphology, transmission electron microscopy (TEM) was used (Hitachi H7600; Hitachi High Technologies America, Schaumburg, IL). PEI gene vector stability was assessed following incubation of DNA-NP in PHP, filtered through Amicon® Ultra Centrifugal Filters (100,000 MWCO), at 37°C. We conducted DLS before and immediately after treatment with PHP as well as at 5 min, 10 min, 20 min and 30 min of incubation. TEM was also conducted immediately after treatment with PHP and at 10 min, 20 min and 30 min of incubation.

FUS-Mediated DNA-BPN Delivery

All sonications were performed using a 1 MHz spherical-face single element FUS transducer with a diameter of 4.5 cm (Olympus, Center Valley, NJ). FUS (0.6 MPa, 120 s, 10 ms bursts, 0.5 Hz burst rate) was targeted to the left striatum. Peak negative pressure was calibrated in de-gassed water using a hydrophone (HGL-0085: bandwidth: 0.5 kHz-40 MHz) and 17-dB preamplifier (GL-0095, Onda Corp., Sunnyvale, CA). The 6-dB acoustic beamwidth along the axial and transverse directions are 15 mm and 4 mm, respectively. The waveform pulsing was driven by a waveform generator (Tektronix AFG310, Bracknell, UK) and amplified using a 55 dB RF power amplifier (ENI 3100LA; Electronic Navigation Industries, Richardson, TX).

Female Sprague-Dawley rats (180-220 g) were anesthetized with an intraperitoneal injection of ketamine (40 mg/kg; Fort Dodge, IA) and dexmedetomidine (0.2 mg/kg, Pfizer, New York, NY) in sterile 0.9% saline. A tail vein catheter was inserted to allow intravenous injections of DNA-BPN and microbubbles. Animal heads were shaved and depilated before being secured prone in a stereotaxic frame (Stoelting, Wood Dale, IL). Rat heads were ultrasonically coupled to a FUS transducer and positioned such that the ultrasound focus was localized to the left striatum. Rats received a co-injection of DNA-BPN (dose based on DNA: 50 μg, 100 μg or 200 μg) and MBs (3×10^5 MBs/g body weight) followed by 0.3 ml of 2% heparinized saline to clear the catheter. Sonication began immediately after clearance of the catheter.

Microbubble Preparation

MBs used in this study are similar to Optison (GE Healthcare, Little Chalfont, Buckinghamshire, UK). To produce MBs, a 1% solution of serum albumin in saline was sonicated (20 kHz, 30 s) with an ultrasound disintegrator (XL2020; Misonix, Farmingdale, NY) with an extended ½-inch titanium probe. The flask containing the solution had its headspace filled with octofluoropropane gas prior to sonication. MBs were sized and counted using a Coulter Counter (Multisizer 3, Beckman Coulter, Fullterton, CA).

In Vivo Bioluminescence Imaging

Animals were anesthetized and maintained on 2-2.5% isofluorane in oxygen. D-Luciferin (Gold Biotechnology, St. Louis, MO) was administered by intraperitoneal injection at 150 mg/kg. Animals were serially imaged using an IVIS100 imaging system (Xenogen, Alameda, CA, USA). Photons were collected and integrated for a period of 1 minute. Images were processed using Xenogen's Living Image software. Total flux intensities were measured from a region of interest over the FUS targeted region.

Ex Vivo Bioluminescence Imaging

Immediately following the final *in vivo* bioluminescence imaging session, rats treated with FUS and DNA-BPN bearing β-actin-luciferase plasmid rats were euthanized and decapitated. The brains were quickly dipped in 10 mg/ml D-luciferin and imaged using the IVIS100 imaging system. Photons emitted were collected over 2 min.

Whole Brain Epifluorescence Imaging

One week after delivery of pBACH-bearing DNA-BPN with FUS, rats were euthanized. Immediately following euthanasia, left and right carotid arteries were cannulated and perfused with 20 ml of 2% heparinized 0.9% saline followed by 10 ml of 4% paraformaldehyde. Brains were immediately placed into 0.9% saline and imaged using an IVIS100 imaging system with the 605 nm excitation and 650 nm emission filters.

Histological Processing

Immediately following euthanasia, left and right carotid arteries were cannulated and perfused with 20 ml of 2% heparinized 0.9% saline followed by 10 ml of 4% paraformaldehyde. Brains were suffusion-fixed in 4% paraformaldehyde for 24 h at 4°C prior to desiccation in 30% sucrose for 24 h at 4°C. Desiccated brains were placed in OCT compound for 1 h prior to flash freezing and ultimate storage at −80°C. Brains were mounted with OCT and sectioned in a cryostat (Leica, Buffalo Grove, IL). Transverse 8 μm thick sections were mounted and stained.

Histology

Hematoxylin and Eosin (H&E) staining was performed on mounted sections according to standard protocols. Tissues were imaged on a bright field microscope (Zeiss, Jena, Germany) equipped with a color CCD Camera (Olympus, Center Valley, NJ).

Immunofluorescence

Mounted sections were washed 3× for 10 min in phosphate buffered saline (PBS) then incubated with blocking solution (Vector Labs, Burlingame, CA). Next, sections were incubated overnight at 4°C with mouse anti-mCherry (1:200; Abcam, Cambridge, MA). After washing 3× for 10 min in PBS, sections were incubated for 1 h at room temperature with Alexafluor-488 conjugated goat anti-mouse IgG (1:250; Invitrogen, Grand Island, NY) and Draq5 (1:1000; Thermo Scientific, Waltham, MA). After washing 3× for 10 min in PBS, slides were mounted using Prolong Gold (Invitrogen) and a coverslip. Sections were imaged on a Nikon Eclipse TE2000 confocal microscope (Nikon, Melville, NY) equipped with a 20× oil objective. Transfection efficiency was assessed using ImageJ by manually counting Draq5+ cells and comparing this to Draq5+ mCherry+ cells. At least three representative fields of view were counted from at least three different section depths within the rat brain.

To assess cell tropism, mounted sections were washed 3× for 10 min in PBS and incubated with blocking solution (Vector Labs, Burlingame, CA). Sections were next incubated overnight with mouse anti-mCherry (1:200; Abcam). After washing 3× for 10 min in PBS, sections were incubated for 1 hr at room temp with Alexa Fluor 647 conjugated goat anti-mouse IgG (Invitrogen). After washing 3× for 10 min in PBS, sections were incubated with mouse anti-glial fibrillary acidic protein (GFAP) (1:500; Millipore Corp.) and mouse anti-neuronal nuclear antigen (NeuN) (1:500; Millipore Corp.). After washing 3× for 10 min in PBS, sections were mounted using Prolong Gold (Invitrogen). Sections were imaged on a Nikon Eclipse TE2000 confocal microscope equipped with a 20× oil objective. Cellular tropism was assessed using ImageJ by manually comparing localization of mCherry+ cells with NeuN+ cells and GFAP+ cells. At least three representative fields of view were counted from at least three different section depths within the rat brain.

Supplementary Material

Refer to Web version on PubMed Central for supplementary material.

Acknowledgements

Funding Sources

Supported by NIH CA164789, NIH EB016784, NIH R01 CA197111, NIH R01 EB020147, NHLBI 5 T32 HL007284 and the Focused Ultrasound Foundation.

ABBREVIATIONS

FUS	Focused ultrasound
DNA-BPN	gene-bearing brain penetrating nanoparticles
NP	nanoparticle
PEG	polyethylene glycol
MB(s)	microbubble(s)
BBB	blood brain barrier
CNS	central nervous system
GFAP	glial cell fibrillary acidic protein
NeuN	Neuronal nuclear antigen
AAV	adeno-associated virus
MR	magnetic resonance

REFERENCES

[1]. Ramaswamy S, McBride JL, Han I, Berry-Kravis EM, Zhou L, Herzog CD, et al. Intrastriatal CERE-120 (AAV-Neurturin) protects striatal and cortical neurons and delays motor deficits in a transgenic mouse model of Huntington’s disease. Neurobiol. Dis. 2009; 34:40–50. doi:10.1016/j.nbd.2008.12.005. [PubMed: 19150499]

[2]. Tereshchenko J, Maddalena A, Bähr M, Kügler S. Pharmacologically controlled, discontinuous GDNF gene therapy restores motor function in a rat model of Parkinson’s disease. Neurobiol. Dis. 2014; 65:35–42. doi:10.1016/j.nbd.2014.01.009. [PubMed: 24440408]

[3]. Bäck S, Peränen J, Galli E, Pulkkila P, Lonka-Nevalaita L, Tamminen T, et al. Gene therapy with AAV2-CDNF provides functional benefits in a rat model of Parkinson's disease. Brain Behav. 2013; 3:75–88. doi:10.1002/brb3.117. [PubMed: 23532969]

[4]. Bjorklund T, Kordower JH. Gene therapy for Parkinson's disease. Mov. Disord. 2010; 25(Suppl 1):S161–73. doi:10.1002/mds.22785. [PubMed: 20187249]

[5]. LeWitt, P. a; Rezai, AR.; Leehey, M. a; Ojemann, SG.; Flaherty, AW.; Eskandar, EN., et al. AAV2-GAD gene therapy for advanced Parkinson's disease: a double-blind, sham-surgery controlled, randomised trial. Lancet Neurol. 2011; 10:309–19. doi:10.1016/S1474-4422(11)70039-4. [PubMed: 21419704]

[6]. Eberling JL, Kells AP, Pivirotto P, Beyer J, Bringas J, Federoff HJ, et al. Functional effects of AAV2-GDNF on the dopaminergic nigrostriatal pathway in parkinsonian rhesus monkeys. Hum. Gene Ther. 2009; 20:511–8. doi:10.1089/hum.2008.201. [PubMed: 19254173]

[7]. Mandel RJ. CERE-110, an adeno-associated virus-based gene delivery vector expressing human nerve growth factor for the treatment of Alzheimer's disease. Curr. Opin. Mol. Ther. 2010; 12:240–247. [PubMed: 20373268]

[8]. Murphy SR, Chang CCY, Dogbevia G, Bryleva EY, Bowen Z, Hasan MT, et al. Acat1 Knockdown Gene Therapy Decreases Amyloid-in a Mouse Model of Alzheimer ' s Disease. Mol. Ther. 2013; 21:1497–1506. doi:10.1038/mt.2013.118. [PubMed: 23774792]

[9]. Mccurdy VJ, Rockwell HE, Arthur JR, Bradbury AM, Johnson AK, Randle AN, et al. Widespread correction of central nervous system disease after intracranial gene therapy in a feline model of Sandhoff disease. Gene Ther. 2014; 22:181–189. doi:10.1038/gt.2014.108. [PubMed: 25474439]

[10]. Berry M, Barrett L, Seymour L, Baird A, Logan A. Gene therapy for central nervous system repair. Curr. Opin. Mol. Ther. 2001; 3:338–349. [PubMed: 11525557]

[11]. Ning J, Wakimoto H. Oncolytic herpes simplex virus-based strategies: Toward a breakthrough in glioblastoma therapy. Front. Microbiol. 2014; 5:1–13. doi:10.3389/fmicb.2014.00303. [PubMed: 24478763]

[12]. Kantor B, McCown TJ, Leone P, Gray SJ. Clinical Applications Involving CNS Gene Transfer. Elsevier. 2014 doi:10.1016/B978-0-12-800149-3.00002-0.

[13]. Bergen JM, Park IK, Horner PJ, Pun SH. Nonviral approaches for neuronal delivery of nucleic acids. Pharm. Res. 2008; 25:983–998. doi:10.1007/s11095-007-9439-5. [PubMed: 17932730]

[14]. Peden CS, Burger C, Muzyczka N, Mandel RJ. Circulating Anti-Wild-Type Adeno-Associated Virus Type 2 (AAV2) Antibodies Inhibit Recombinant AAV2 (rAAV2)-Mediated, but Not rAAV5-Mediated, Gene Transfer in the Brain. J. Virol. 2004; 78:6344–6359. doi:10.1128/JVI.78.12.6344. [PubMed: 15163728]

[15]. Calcedo R, Wilson JM. Humoral Immune Response to AAV. Front. Immunol. 2013; 4:341. doi:10.3389/fimmu.2013.00341. [PubMed: 24151496]

[16]. Pardridge WM. The blood-brain barrier: bottleneck in brain drug development. NeuroRx. 2005; 2:3–14. doi:10.1602/neurorx.2.1.3. [PubMed: 15717053]

[17]. Deleu D, Northway MG, Hanssens Y. Clinical pharmacokinetic and pharmacodynamic properties of drugs used in the treatment of Parkinson's disease. Clin. Pharmacokinet. 2002; 41:261–309. doi:10.2165/00003088-200241040-00003. [PubMed: 11978145]

[18]. Kroll RA, Neuwelt EA. Outwitting the blood-brain barrier for therapeutic purposes: Osmotic opening and other means. Neurosurgery. 1998; 42:1083–1100. doi:10.1097/00006123-199805000-00082. [PubMed: 9588554]

[19]. Pardridge WM. Blood-brain barrier delivery. Drug Discov. Today. 2007; 12:54–61. doi:10.1016/j.drudis.2006.10.013. [PubMed: 17198973]

[20]. Hynynen K, McDannold NJ. Noninvavie MR Imaging-guided Focal Opening of the Blood-Brain Barrier in Rabbits. Radiology. 2001; 220:640–646. [PubMed: 11526261]

[21]. Nance E, Timbie K, Miller GW, Song J, Louttit C, Klibanov AL, et al. Non-invasive delivery of stealth, brain-penetrating nanoparticles across the blood-brain barrier using MRI-guided focused ultrasound. J. Control. Release. 2014; 189:123–32. doi:10.1016/j.jconrel.2014.06.031. [PubMed: 24979210]

[22]. Hosseinkhah N, Hynynen K. A three-dimensional model of an ultrasound contrast agent gas bubble and its mechanical effects on microvessels. Phys. Med. Biol. 2012; 57:785–808. doi: 10.1088/0031-9155/57/3/785. [PubMed: 22252221]

[23]. Sheikov N, McDannold NJ, Vykhodtseva NI, Jolesz FA, Hynynen K. Cellular mechanisms of the blood-brain barrier opening induced by ultrasound in presence of microbubbles. Ultrasound Med. Biol. 2004; 30:979–89. doi:10.1016/j.ultrasmedbio.2004.04.010. [PubMed: 15313330]

[24]. Shang X, Wang P, Liu Y, Zhang Z. Mechanism of Low-Frequency Ultrasound in Opening Blood – Tumor Barrier by Tight Junction. J Mol Neurosci. 2011; 43:364–369. doi:10.1007/s12031-010-9451-9. [PubMed: 20852968]

[25]. Vlachos F, Tung Y-S, Konofagou EE. Permeability assessment of the focused ultrasound-induced blood-brain barrier opening using dynamic contrast-enhanced MRI. Phys. Med. Biol. 2010; 55:5451–66. doi:10.1088/0031-9155/55/18/012. [PubMed: 20736501]

[26]. McDannold NJ, Arvanitis CD, Vykhodtseva NI, Livingstone MS. Temporary disruption of the blood-brain barrier by use of ultrasound and microbubbles: safety and efficacy evaluation in rhesus macaques. Cancer Res. 2012; 72:3652–63. doi:10.1158/0008-5472.CAN-12-0128. [PubMed: 22552291]

[27]. Hynynen K, McDannold NJ, Sheikov N, Jolesz FA, Vykhodtseva NI. Local and reversible blood-brain barrier disruption by noninvasive focused ultrasound at frequencies suitable for trans-skull sonications. Neuroimage. 2005; 24:12–20. doi:10.1016/j.neuroimage.2004.06.046. [PubMed: 15588592]

[28]. Etame AB, Diaz RJ, Reilly MAO, Smith CA, Mainprize TG, Hynynen K, et al. Enhanced delivery of gold nanoparticles with therapeutic potential into the brain using MRI-guided focused ultrasound, Nanomedicine Nanotechnology. Biol. Med. 2012; 8:1133–1142. doi:10.1016/j.nano.2012.02.003.

[29]. Treat LH, McDannold NJ, Zhang Y, Vykhodtseva NI, Hynynen K. Improved anti-tumor effect of liposomal doxorubicin after targeted blood-brain barrier disruption by MRI-guided focused ultrasound in rat glioma. Ultrasound Med. Biol. 2012; 38:1716–25. doi:10.1016/j.ultrasmedbio.2012.04.015. [PubMed: 22818878]

[30]. Treat LH, McDannold NJ, Vykhodtseva NI, Zhang Y, Tam K, Hynynen K. Targeted delivery of doxorubicin to the rat brain at therapeutic levels using MRI-guided focused ultrasound. Int. J. Cancer. 2007; 121:901–7. doi:10.1002/ijc.22732. [PubMed: 17437269]

[31]. Kinoshita M, McDannold NJ, Jolesz FA, Hynynen K. Noninvasive localized delivery of Herceptin to the mouse brain by MRI-guided focused ultrasound-induced blood-brain barrier disruption. Proc. Natl. Acad. Sci. U. S. A. 2006; 103:11719–23. doi:10.1073/pnas.0604318103. [PubMed: 16868082]

[32]. Jordão JF, Thévenot E, Markham-Coultes K, Scarcelli T, Weng Y-Q, Xhima K, et al. Amyloid-plaque reduction, endogenous antibody delivery and glial activation by brain-targeted, transcranial focused ultrasound. Exp. Neurol. 2013; 248:16–29. doi:10.1016/j.expneurol.2013.05.008. [PubMed: 23707300]

[33]. Wang F, Shi Y, Lu L, Liu L, Cai Y, Zheng H, et al. Targeted delivery of GDNF through the blood-brain barrier by MRI-guided focused ultrasound. PLoS One. 2012; 7:e52925. doi:10.1371/journal.pone.0052925. [PubMed: 23300823]

[34]. Thévenot E, Jordão JF, O'Reilly M. a, Markham K, Weng Y-Q, Foust KD, et al. Targeted delivery of self-complementary adeno-associated virus serotype 9 to the brain, using magnetic resonance imaging-guided focused ultrasound. Hum. Gene Ther. 2012; 23:1144–55. doi:10.1089/hum.2012.013. [PubMed: 22838844]

[35]. Alonso A, Reinz E, Leuchs B, Kleinschmidt J, Fatar M, Geers B, et al. Focal Delivery of AAV2/1-transgenes Into the Rat Brain by Localized Ultrasound-induced BBB Opening. Mol. Ther. Nucleic Acids. 2013; 2:e73. doi:10.1038/mtna.2012.64. [PubMed: 23423361]

[36]. Burgess A, Ayala-Grosso C. a, Ganguly M, Jordão JF, Aubert I, Hynynen K. Targeted delivery of neural stem cells to the brain using MRI-guided focused ultrasound to disrupt the blood-brain barrier. PLoS One. 2011; 6:e27877. doi:10.1371/journal.pone.0027877. [PubMed: 22114718]

[37]. Chen H, Konofagou EE. The size of blood-brain barrier opening induced by focused ultrasound is dictated by the acoustic pressure. J. Cereb. Blood Flow Metab. 2014; 34:1197–1204. doi:10.1038/jcbfm.2014.71. [PubMed: 24780905]

[38]. Dallapiazza R, McKisic MS, Shah B, Elias WJ. Neuromodulation for movement disorders. Neurosurg. Clin. N. Am. 2014; 25:47–58. doi:10.1016/j.nec.2013.08.002. [PubMed: 24262899]

[39]. Elias WJ, Huss D, Voss T, Loomba J, Khaled M, Zadicario E, et al. A pilot study of focused ultrasound thalamotomy for essential tremor. N. Engl. J. Med. 2013; 369:640–8. doi:10.1056/NEJMoa1300962. [PubMed: 23944301]

[40]. Nance E, Woodworth GF, Sailor K, Shih T-Y, Xu Q, Swaminathan G, et al. A dense poly(ethylene glycol) coating improves penetration of large polymeric nanoparticles within brain tissue. Sci. Transl. Med. 2012; 4:149ra119. doi:10.1126/scitranslmed.3003594.

[41]. Kenny GD, Bienemann AS, Tagalakis AD, Pugh J. a. Welser K, Campbell F, et al. Multifunctional receptor-targeted nanocomplexes for the delivery of therapeutic nucleic acids to the Brain. Biomaterials. 2013; 34:9190–9200. doi:10.1016/j.biomaterials.2013.07.081. [PubMed: 23948162]

[42]. Bobo RH, Laske DW, Akbasak A, Morrisont PF, Dedrickt RL, Oldfield EH. Convection-enhanced delivery of macromolecules in the brain. Proc. Natl. Acad. Sci. 1994; 91:2076–2080. [PubMed: 8134351]

[43]. Mastorakos P, Zhang C, Berry S, Oh Y, Lee S, Eberhart CG, et al. Highly PEGylated DNA Nanoparticles Provide Uniform and Widespread Gene Transfer in the Brain. Adv. Healthc. Mater. 2015 n/a-n/a. doi:10.1002/adhm.201400800.

[44]. Burke CW, Suk JS, Kim AJ, Hsiang Y-HJ, Klibanov AL, Hanes J, et al. Markedly Enhanced Skeletal Muscle Transfection Achieved by the Ultrasound-Targeted Delivery of Non-Viral Gene Nanocarriers with Microbubbles. J. Control. Release. 2012; 162:414–421. doi:10.1016/j.jconrel.2012.07.005. [PubMed: 22800583]

[45]. Boylan NJ, Suk JS, Lai SK, Jelinek R, Boyle MP, Cooper MJ, et al. Highly compacted DNA nanoparticles with low MW PEG coatings: in vitro, ex vivo and in vivo evaluation. J. Control. Release. 2012; 157:72–9. doi:10.1016/j.jconrel.2011.08.031. [PubMed: 21903145]

[46]. Merkel OM, Urbanics R, Bedocs P, Rozsnyay Z, Rosivall L, Toth M, et al. In vitro and in vivo complement activation and related anaphylactic effects associated with polyethylenimine and polyethylenimine-graft-poly(ethylene glycol) block copolymers. Biomaterials. 2011; 32:4936–4942. doi:10.1016/j.biomaterials.2011.03.035. [PubMed: 21459440]

[47]. Malek A, Czubayko F, Aigner A. PEG grafting of polyethylenimine (PEI) exerts different effects on DNA transfection and siRNA-induced gene targeting efficacy. J. Drug Target. 2008; 16:124–139. doi:10.1080/10611860701849058. [PubMed: 18274933]

[48]. Petersen H, Fechner PM, Martin AL, Kunath K, Stolnik S, Roberts CJ, et al. Polyethylenimine-graft-poly(ethylene glycol) copolymers: Influence of copolymer block structure on DNA complexation and biological activities as gene delivery system. Bioconjug. Chem. 2002; 13:845–854. doi:10.1021/bc025529v. [PubMed: 12121141]

[49]. Thomas CE, Storm T. a, Huang Z, Kay M. a. Rapid uncoating of vector genomes is the key to efficient liver transduction with pseudotyped adeno-associated virus vectors. J. Virol. 2004; 78:3110–3122. doi:10.1128/JVI.78.6.3110-3122.2004. [PubMed: 14990730]

[50]. Miao CH, Snyder RO, Schowalter DB, Patijn G, Donahue B, Winther B, et al. The Kinetics of rAAV Integration in the Liver. Nat. Genet. 1998; 18:231–236. doi:10.1038/ng0598-51. [PubMed: 9500544]

[51]. Huang Q, Deng J, Xie Z, Wang F, Chen S, Lei B, et al. Effective Gene Transfer into Central Nervous System Following Ultrasound-Microbubbles-Induced Opening of the Blood-Brain Barrier. Ultrasound Med. Biol. 2012; 38:1234–1243. doi:10.1016/j.ultrasmedbio.2012.02.019. [PubMed: 22677255]

[52]. Burke CW, Alexander E, Timbie K, Kilbanov AL, Price RJ. Ultrasound-activated Agents Comprised of 5FU-bearing Nanoparticles Bonded to Microbubbles Inhibit Solid Tumor Growth and Improve Survival. Mol. Ther. 2014; 22:321–8. doi:10.1038/mt.2013.259. [PubMed: 24172867]

[53]. Burke CW, Hsiang Y-HJHJ, Alexander E, Kilbanov AL, Price RJ, Alexander E IV, et al. Covalently linking poly(lactic-co-glycolic acid) nanoparticles to microbubbles before intravenous injection improves their ultrasound-targeted delivery to skeletal muscle. Small. 2011; 7:1227–35. doi:10.1002/smll.201001934. [PubMed: 21456081]

[54]. Drinkut A, Tereshchenko Y, Schulz JB, Bähr M, Kügler S. Efficient gene therapy for Parkinson's disease using astrocytes as hosts for localized neurotrophic factor delivery. Mol. Ther. 2012; 20:534–43. doi:10.1038/mt.2011.249. [PubMed: 22086235]

[55]. Wang S, Olumolade OO, Sun T, Samiotaki G, Konofagou EE. Noninvasive, neuron-specific gene therapy can be facilitated by focused ultrasound and recombinant adeno-associated virus. Gene Ther. 2014:1–7. doi:10.1038/gt.2014.91.

[56]. Gray SJ, Foti SB, Schwartz JW, Bachaboina L, Taylor-Blake B, Coleman J, et al. Optimizing promoters for recombinant adeno-associated virus-mediated gene expression in the peripheral and central nervous system using self-complementary vectors. Hum. Gene Ther. 2011; 22:1143–53. doi:10.1089/hum.2010.245. [PubMed: 21476867]

[57]. Allen SJ, Watson JJ, Shoemark DK, Barua NU, Patel NK. GDNF, NGF and BDNF as therapeutic options for neurodegeneration. Pharmacol. Ther. 2013; 138:155–75. doi:10.1016/j.pharmthera.2013.01.004. [PubMed: 23348013]

[58]. Hidalgo-Figueroa M, Bonilla S, Gutierrez F, Pascual a. Lopez-Barneo J. GDNF Is Predominantly Expressed in the PV+ Neostriatal Interneuronal Ensemble in Normal Mouse and after Injury of the Nigrostriatal Pathway. J. Neurosci. 2012; 32:864–872. doi:10.1523/JNEUROSCI.2693-11.2012. [PubMed: 22262884]

[59]. Rodríguez JJ, Verkhratsky A. Neuroglial roots of neurodegenerative diseases? Mol. Neurobiol. 2011; 43:87–96. doi:10.1007/s12035-010-8157-x. [PubMed: 21161612]

[60]. Davila D, Thibault K, Fiacco T. a, Agulhon C. Recent molecular approaches to understanding astrocyte function in vivo. Front. Cell. Neurosci. 2013; 7:272. doi:10.3389/fncel.2013.00272. [PubMed: 24399932]

[61]. Rodrigues RWP, Gomide VC, Chadi G. Astroglial and microglial activation in the wistar rat ventral tegmental area after a single striatal injection of 6-hydroxydopamine. Int. J. Neurosci. 2004; 114:197–216. doi:10.1080/00207450490249338\rXU1HKG7C0W22PD36 [pii]. [PubMed: 14702208]

[62]. O'Callaghan JP, Miller DB. The concentration of glial fibrillary acidic protein increases with age in the mouse and rat brain. Neurobiol. Aging. 1991; 12:171–4. http://www.ncbi.nlm.nih.gov/pubmed/1904995. [PubMed: 1904995]

[63]. Duque S, Joussemet B, Riviere C, Marais T, Dubreil L, Douar A-M, et al. Intravenous administration of self-complementary AAV9 enables transgene delivery to adult motor neurons. Mol. Ther. 2009; 17:1187–1196. doi:10.1038/mt.2009.71. [PubMed: 19367261]

[64]. Weber-Adrian D, Thévenot E, O'Reilly M. a, Oakden W, Akens MK, Ellens N, et al. Gene delivery to the spinal cord using MRI-guided focused ultrasound. Gene Ther. 2015 doi:10.1038/gt.2015.25.

[65]. Wu J, Zhao W, Zhong L, Han Z, Li B, Ma W, et al. Self-complementary recombinant adeno-associated viral vectors: packaging capacity and the role of rep proteins in vector purity. Hum. Gene Ther. 2007; 18:171–182. doi:10.1089/hum.2006.088. [PubMed: 17328683]

[66]. Lin C-Y, Hsieh H-Y, Pitt WG, Huang C-Y, Tseng I-C, Yeh C-K, et al. Focused Ultrasound-Induced Blood-Brain Barrier Opening for Non-Viral, Non-invasive, and Targeted Gene Delivery. J. Control. Release. 2015; 212:1–9. doi:10.1016/j.jconrel.2015.06.010. [PubMed: 26071631]

[67]. Tung Y-S, Vlachos F, Feshitan J, Borden M, Konofagou EE. The mechanism of interaction between focused ultrasound and microbubbles in blood-brain barrier opening in mice. J. Acoust. Soc. Am. 2011; 130:3059. doi:10.1121/1.3646905. [PubMed: 22087933]

[68]. McDannold NJ, Vykhodtseva NI, Hynynen K. Targeted disruption of the blood-brain barrier with focused ultrasound: association with cavitation activity. Phys. Med. Biol. 2006; 51:793–807. doi:10.1088/0031-9155/51/4/003. [PubMed: 16467579]

[69]. McDannold NJ, Vykhodtseva NI, Raymond S, Jolesz FA, Hynynen K. MRI-guided targeted blood-brain barrier disruption with focused ultrasound: Histological findings in rabbits. Ultrasound Med. Biol. 2005; 31:1527–1537. doi:10.1016/j.ultrasmedbio.2005.07.010. [PubMed: 16286030]

[70]. Godbey WT, Wu KK, Mikos AG. Poly(ethylenimine) and its role in gene delivery. J. Control. Release. 1999; 60:149–160. doi:10.1016/S0168-3659(99)00090-5. [PubMed: 10425321]

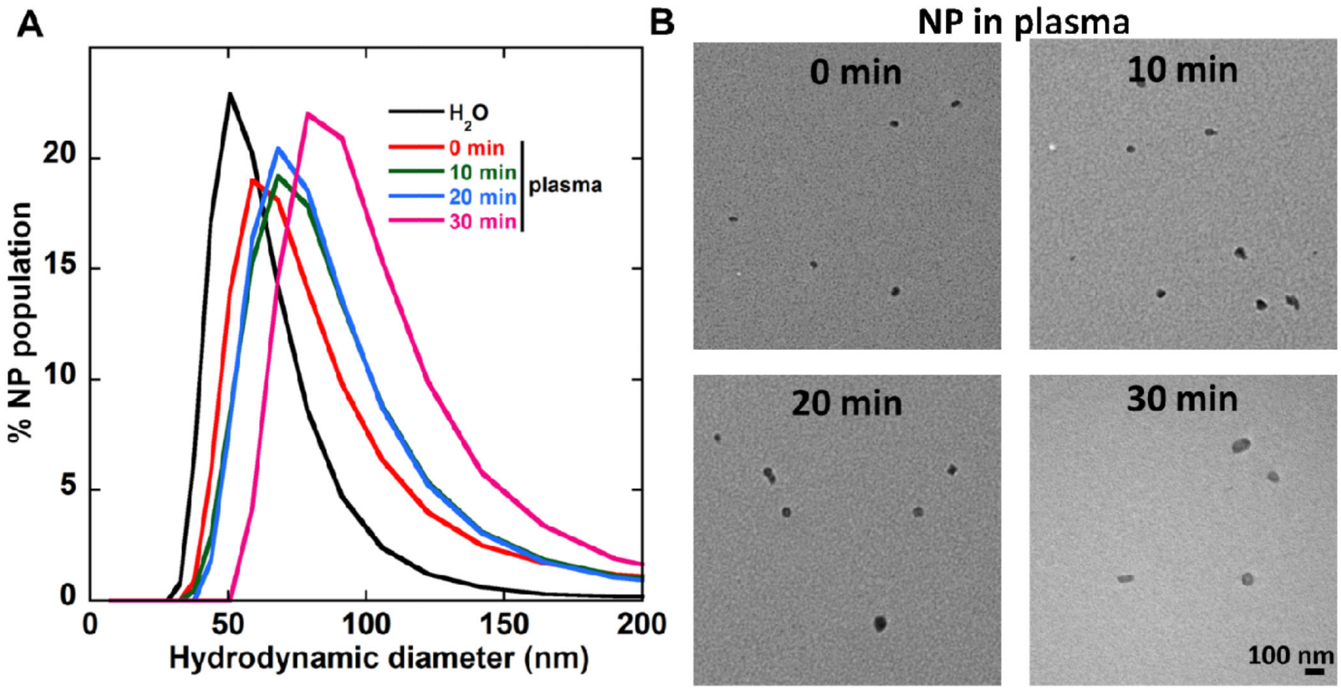

Figure 1.

DNA-BPN stability in PHP (A) Gene vector hydrodynamic diameter (number mean) distribution following incubation in PHP at 37°C for 0, 10, 20 and 30 min. Size was measured by DLS in 10 mM NaCl at pH 7.0. (B) Transmission electron microscopy images of gene vectors following incubation in PHP at 37°C. Scale bar: 100 nm.

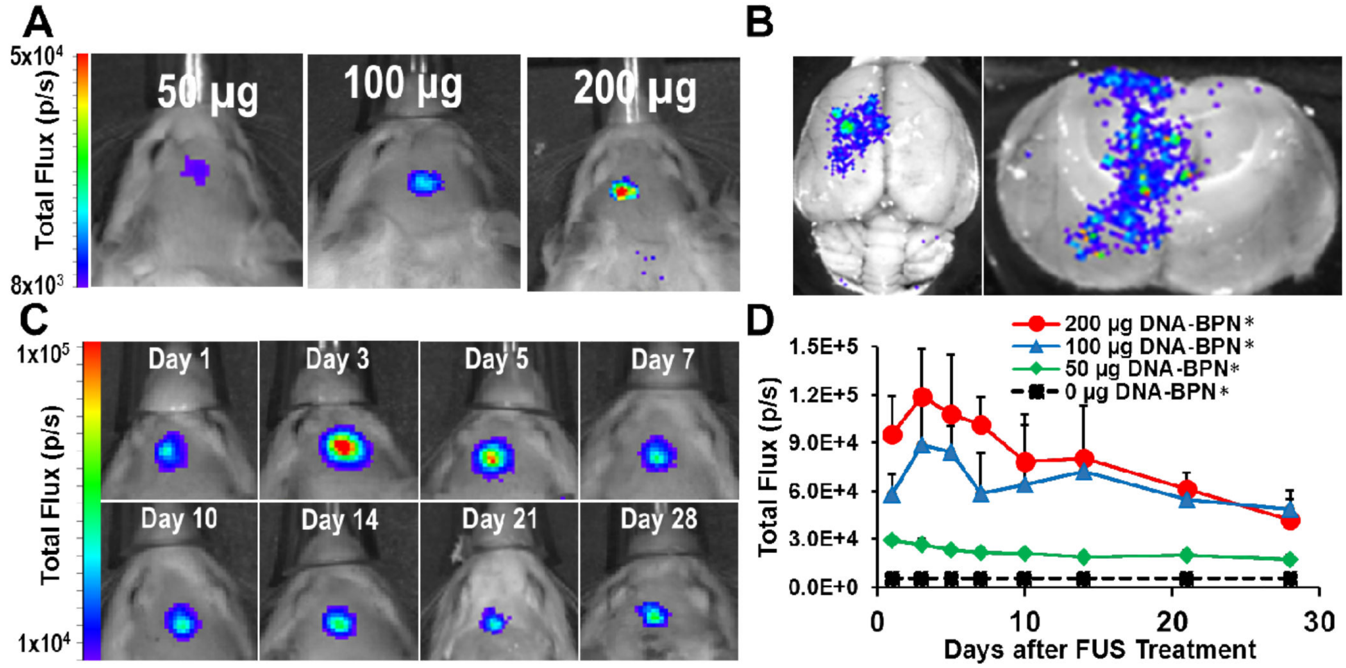

Figure 2.

FUS-mediated delivery of pBAL DNA-BPN across the BBB leads to robust and localized transgene expression in the rat brain. (A) Representative IVIS bioluminescence scans acquired 7 days after delivery of luciferase-bearing DNA-BPN into the rat brain with FUS. Bioluminescence was dependent on the DNA-BPN dose. (B) *Ex vivo* bioluminescence IVIS scans showing transgene distribution through axial plane (left) and coronal plane (right) 28 days after FUS treatment. (C) Representative IVIS bioluminescence images in a rat given 200 µg luciferase bearing DNA-BPN over 28 days. (D) Line graph of bioluminescence total flux over the 28 day test period. n = 5 at each dose. *Significantly different than all other doses tested ($p<0.05$).

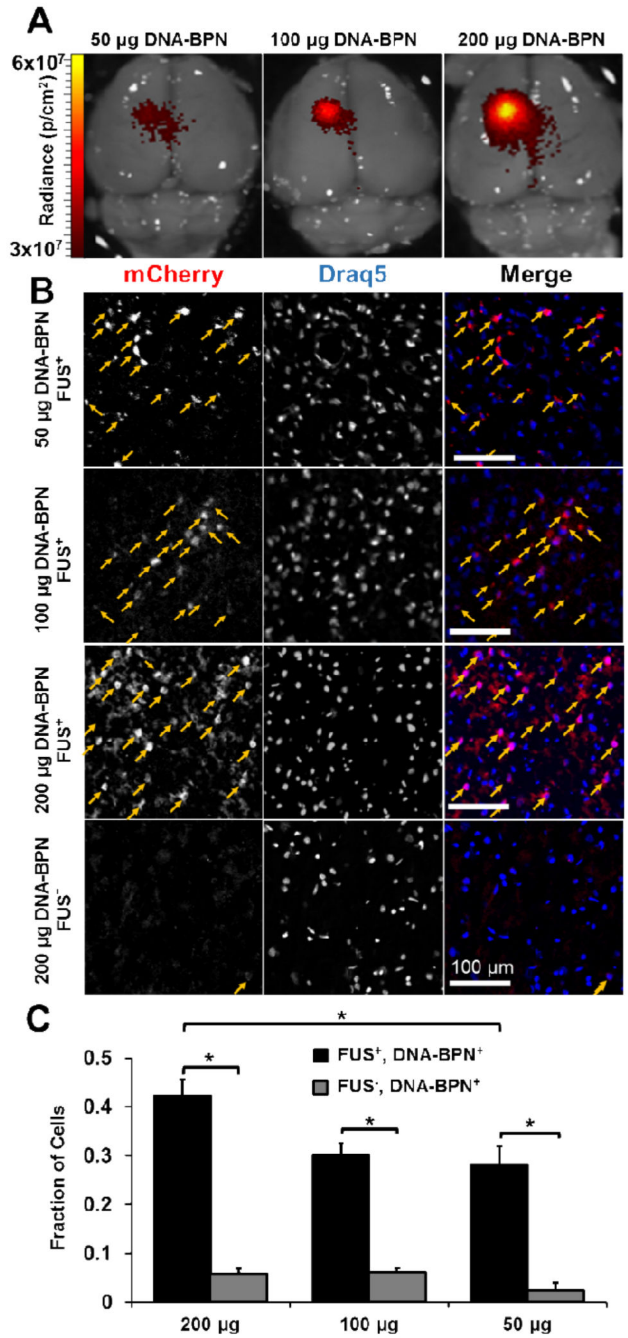

Figure 3.

FUS mediated delivery of pBACH DNA-BPN into rat brain leads to efficient and localized transfection. (A) Representative whole brain *ex vivo* epifluorescence IVIS scans taken 7 days after delivery of DNA-BPN. (B) Confocal fluorescence images show mCherry (red, left column), Draq5 (blue, middle column) and merge (right column) images 7 days after FUS-mediated delivery of DNA-BPN. Arrows indicate co-localization of mCherry and Draq5. Scale bar = 100 um. (C) Bar graphs showing transfection efficiency 7 days after

DNA-BPN delivery with FUS compared to contralateral non-FUS treated hemisphere. n = 6 per dose. * Significantly different ($p<0.05$).

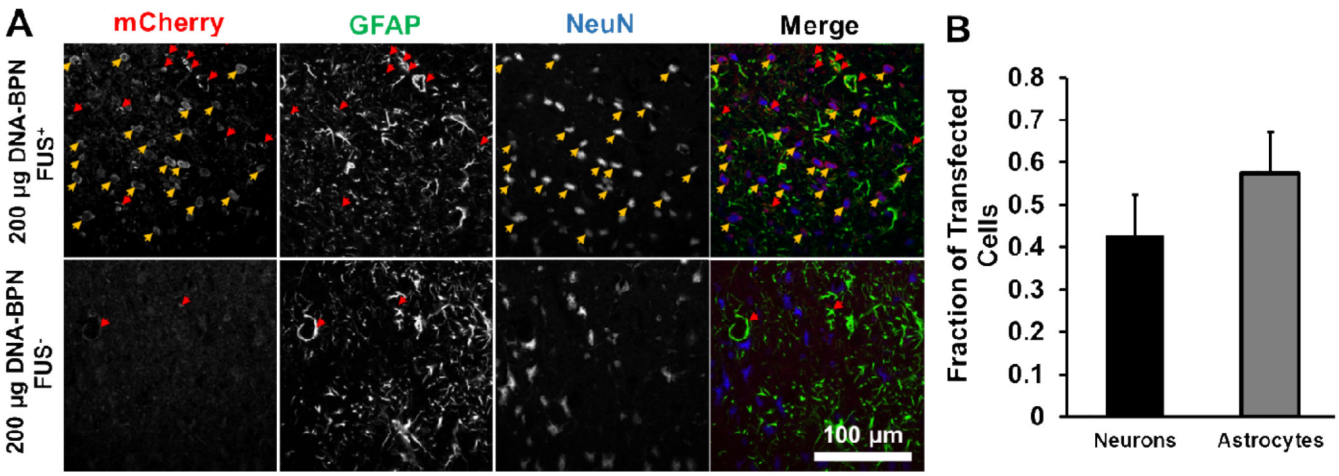

Figure 4.

DNA-BPN delivered across the BBB with FUS transfect both astrocytes and neurons. (A) Representative confocal fluorescent images show mCherry (red, left column), GFAP (green, middle-left column), NeuN (blue, middle-right column), and merge (right column) images 7 days after delivery of pBACH DNA-BPN with FUS (top row) or without FUS (bottom row). Arrows indicate colocalization of mCherry and GFAP (red) or NeuN (yellow). Scale bar = 100 µm. (B) Bar graph showing the relative fraction of mCherry^{+} cells that colocalize with the GFAP astrocytic marker or the NeuN neuronal marker. n = 6.

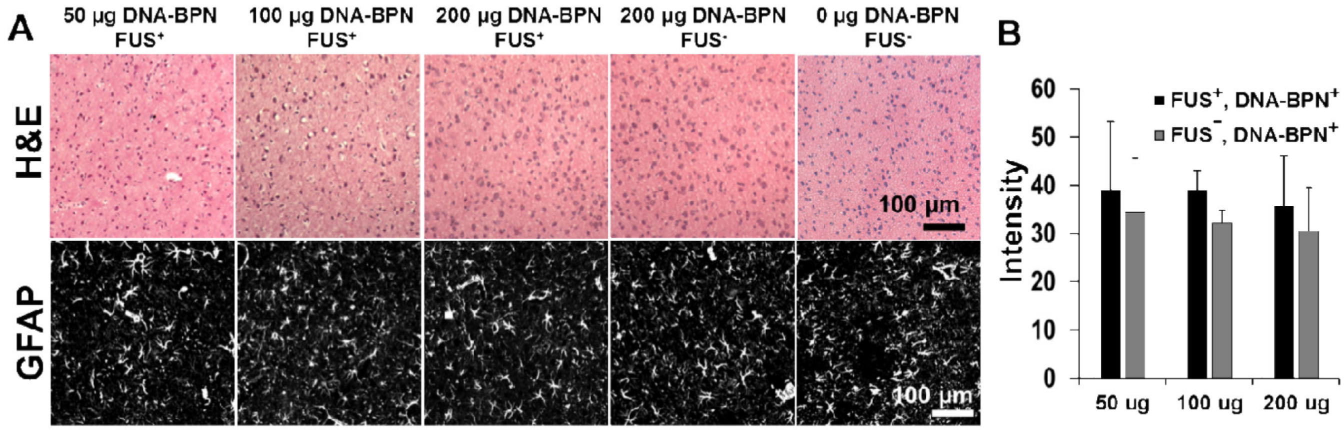

Figure 5.

Examination of brain tissues for toxicity and gliosis at 1 week after DNA-BPN delivery with FUS. (A) Representative images from n=6 per dose H&E-stained sections (top) or confocal GFAP-immunofluorescence sections 7 days after DNA-BPN delivery with FUS. No signs of toxicity were found in brains treated with FUS and DNA-BPN. Hemosiderin staining was found in 11% of n=18 brains tested. (B) Bar graph of GFAP grayscale intensity in the FUS^+ and DNA-BPN treated regions as well as the contralateral FUS^- hemisphere. n=6 per dose. No statistical differences were found.

Author Manuscript

Author Manuscript

Author Manuscript

Table 1

Physiochemical properties of DNA-BPN.

	Hydrodynamic Diameter ± SEM (nm)[a]		ζ-potential ± SEM (mV)[b]	PDI[a]
	Number mean	z-average		
DNA-BPN	56 ± 2	106 ± 1	1.5 ± 0.3	0.18
DNA-BPN in plasma [c]	65 ± 7	130 ± 2	−1.8 ± 0.8	0.25

[a]Size and PDI were measured by DLS in 10 mM NaCl at pH 7.0 and data are presented as the average of at least 3 measurements ± standard error of the mean (SEM).

[b]ζ-potential was similarly measured by laser Doppler anemometry and data are presented as the average of at least 3 measurements ± SEM.

[c]Physicochemical characteristics were measured following 5 min incubation in PHP at 37°C.